

Dendritic organization of sensory input to cortical neurons *in vivo*

Hongbo Jia^{1*}, Nathalie L. Rochefort^{1*}, Xiaowei Chen¹ & Arthur Konnerth¹

In sensory cortex regions, neurons are tuned to specific stimulus features. For example, in the visual cortex, many neurons fire predominantly in response to moving objects of a preferred orientation. However, the characteristics of the synaptic input that cortical neurons receive to generate their output firing pattern remain unclear. Here we report a novel approach for the visualization and functional mapping of sensory inputs to the dendrites of cortical neurons *in vivo*. By combining high-speed two-photon imaging with electrophysiological recordings, we identify local subthreshold calcium signals that correspond to orientation-specific synaptic inputs. We find that even inputs that share the same orientation preference are widely distributed throughout the dendritic tree. At the same time, inputs of different orientation preference are interspersed, so that adjacent dendritic segments are tuned to distinct orientations. Thus, orientation-tuned neurons can compute their characteristic firing pattern by integrating spatially distributed synaptic inputs coding for multiple stimulus orientations.

A growing amount of evidence indicates that information processing in the brain involves the computation of electrical and chemical signals in neuronal dendrites (for a review, see ref. 1). One of the most effective ways for the analysis of these dendritic signals relies on the imaging of the dynamics of intracellular Ca^{2+} concentration (reviewed in ref. 2). Thus, synaptic input-related dendritic Ca^{2+} transients have been identified and studied in detail *in vitro*^{3–6}, while *in vivo* work has explored action-potential-related dendritic Ca^{2+} signals^{7–9}. However, nothing is known about the nature of subthreshold sensory evoked input signals in the dendrites of mammalian cortical neurons. A detailed knowledge of sensory input signals would represent an important step forward in the understanding of dendritic computation^{1,10–13}. An intriguing open question is whether sensory inputs with similar features are clustered on the same dendrite of a neuron or dispersed throughout the dendritic tree. Clustered inputs are capable of generating dendritic spikes (reviewed in ref. 11) and may form neuronal computational subunits *in vivo*, as they do under certain experimental conditions *in vitro*¹⁴. Alternatively, sensory inputs that are not clustered, but widely distributed, may underlie different rules of integration and formation of neuronal output signals—like, for example, the linear summation of excitatory inputs¹⁵.

Visually evoked supra- and subthreshold activity

For the functional analysis of spiny dendrites *in vivo* by means of two-photon calcium imaging, we selected as an experimental model neurons in layer 2/3 of the mouse primary visual cortex (Fig. 1a–c). The somata of the neurons were located approximately between 140 and 200 μm below the cortical surface. Their dendritic trees had a characteristic pattern, consisting of numerous basal and oblique dendrites but no pronounced apical trunk^{16–18} (Fig. 1a). As in many other mammalian species^{19–21}, layer 2/3 neurons of the mouse primary visual cortex respond selectively to drifting gratings or bars with action potential firing^{22–24}. By performing whole-cell recordings involving the ‘shadow-patching’ approach²⁵, we found that stimulation with drifting gratings shifted the membrane potential to the ‘up-state’²⁶

for the entire duration of the stimulus. An increased probability of up-states during drifting grating stimulation was previously observed in the cat visual cortex²⁷. The neuron illustrated in Fig. 1d fired action potentials preferentially during the presentation of specifically oriented drifting gratings and was identified as a ‘highly-tuned’ neuron (Fig. 1e left) on the basis of its orientation selectivity index (OSI), which was higher than 0.5 (Methods). In our recordings, 6 out of 17 neurons were highly tuned for a preferred orientation (Fig. 1f left), 6/17 neurons were poorly tuned, while the rest of 5/17 neurons did not respond reliably to visual stimulation. For a better assessment of the stimulus-evoked subthreshold depolarization in highly tuned neurons, we hyperpolarized them to subthreshold membrane potentials. In the example shown in Fig. 1d, the neuron was hyperpolarized from its resting level of -64 mV to -70 mV. In contrast to the highly tuned action potential pattern (Fig. 1e left), the stimulus-evoked subthreshold depolarizing responses were broadly tuned in this (Fig. 1e right) as well as in all other highly tuned neurons (Fig. 1f right). Thus, in mouse visual cortex, as in cat visual cortex^{28,29}, the high tuning level of action potential firing, the neuronal output signal, contrasts with the low tuning level of the afferent subthreshold input signals.

These observations prompted us to combine whole-cell recordings with two-photon calcium imaging to search for dendritic signals associated with the afferent activity. We performed high-speed two-photon imaging at 30 full frames per second or 60 half frames per second using resonant galvo-scanners³⁰ and, initially, focused on the dendrites that were visible in the plane of focus containing the cell body (Fig. 1g). When stimulated with their preferred orientation, neurons responded with action potential firing that was associated with global dendritic calcium transients in all imaged dendrites. In the neuron illustrated in Fig. 1g, all five visible dendrites displayed calcium transients that were larger when the neuron fired four action potentials (Fig. 1h left) than when it fired two action potentials (Fig. 1h right). The dependence of the calcium transient amplitude on the number of action potentials and the observation that similar calcium transients were evoked by direct neuronal depolarization through the recording pipette (Supplementary Fig. 1a–c) indicate

¹Institute of Neuroscience and Center for Integrated Protein Science, Technical University Munich, Biedersteinerstrasse 29, 80802 Munich, Germany.

*These authors contributed equally to this work.

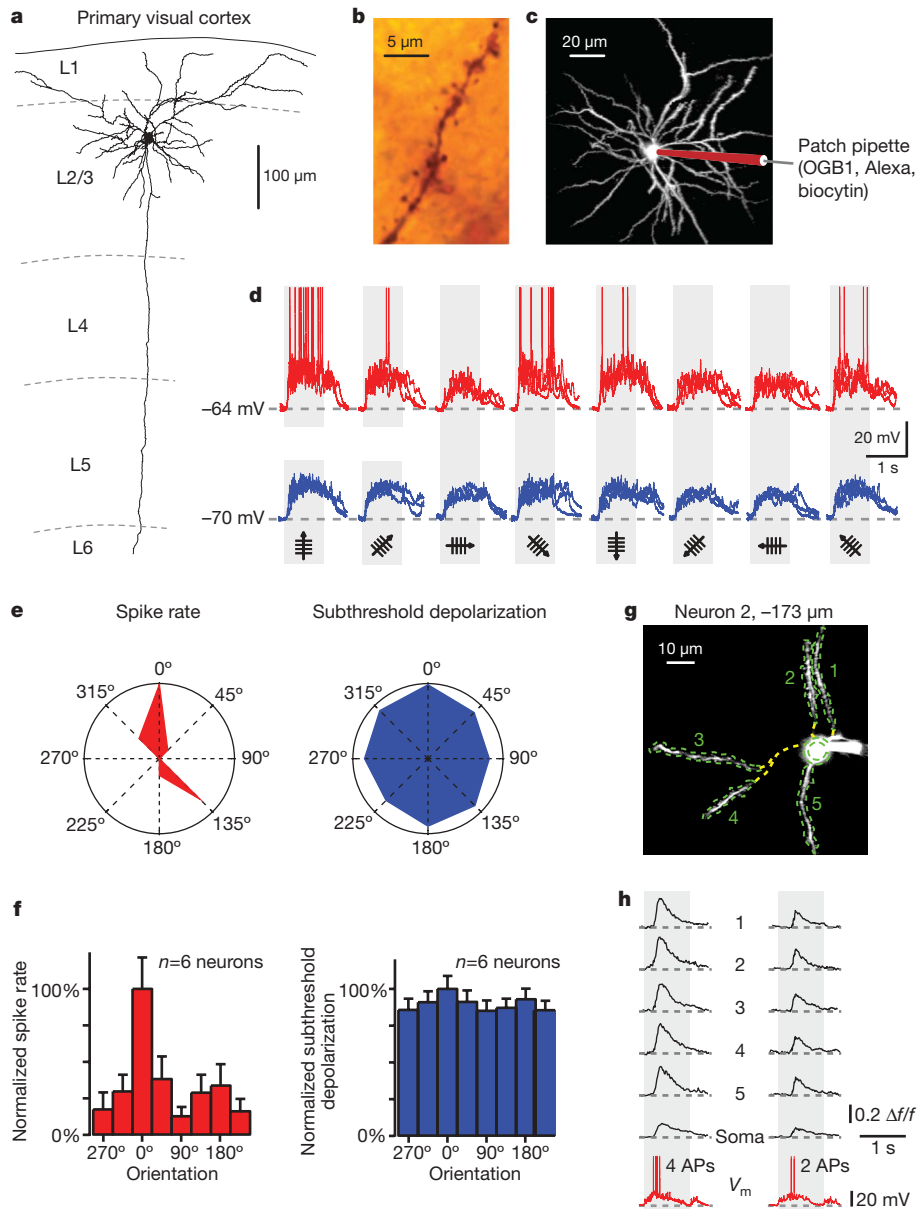


Figure 1 | Visually evoked action potentials, subthreshold depolarizations and global dendritic calcium signals. **a**, Reconstruction of a biocytin-filled layer 2/3 (L2/3) neuron in mouse primary visual cortex (projection along the antero-posterior axis). Data from the same neuron are presented in **b–e**. **b**, Microphotograph of a spiny basal dendrite. **c**, Projection along the dorso-ventral axis obtained *in vivo* from 469 sections (step size 0.5 μm) from Alexa fluorescence. **d**, Whole-cell current-clamp recordings of responses to drifting gratings of different orientations. Three trials were superimposed. Upper red traces, action potential responses at resting potential (indicated on the left); lower blue traces, subthreshold responses obtained after hyperpolarizing the neuron to -70 mV. **e**, Polar plots of visually evoked responses, average of eight trials. Red plot, spike rate; blue plot, amplitude of subthreshold depolarization. **f**, Tuning properties of spiking and

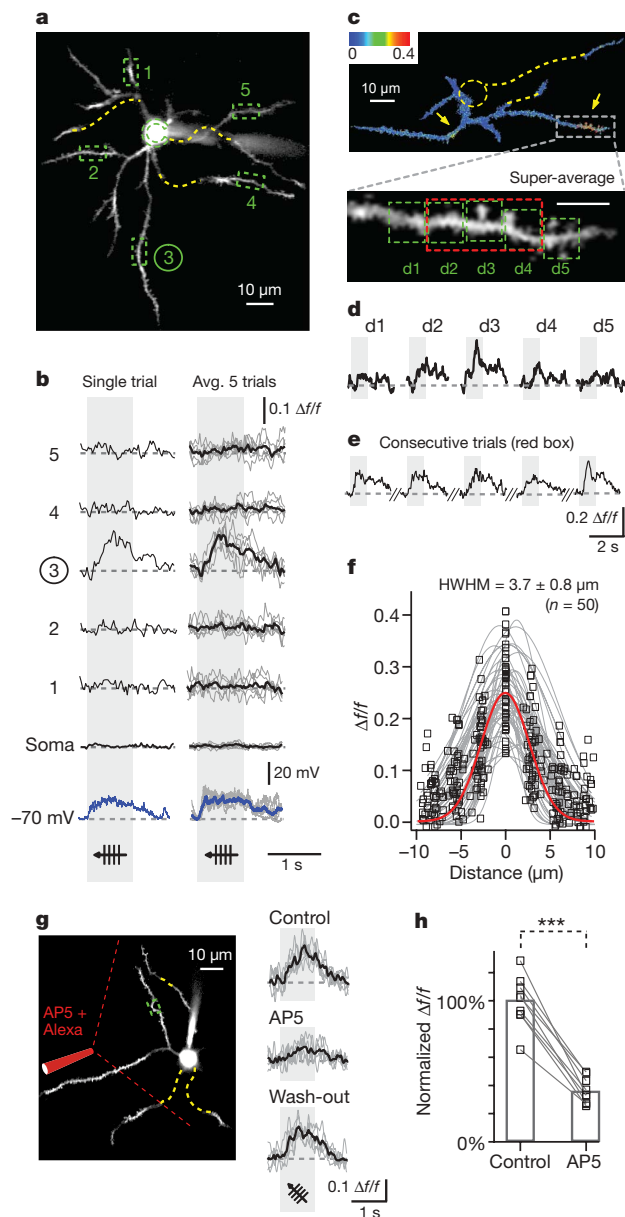
that such global dendritic signals are largely due to the activation of voltage-gated calcium channels by back-propagating action potentials; this has previously been shown for basal dendrites in *in vitro* recordings from layer 2/3 neurons^{31,32}. The amplitude of the Ca^{2+} transients at different dendritic sites showed attenuation along a given dendrite (Supplementary Fig. 1d, e) and variations from trial to trial, but we were unable to obtain unambiguous evidence for signal peaks that would correspond to specific synaptic inputs, as found in tectal neurons of the tadpole³³. Therefore, we decided to search for calcium signals associated with subthreshold synaptic

subthreshold responses for six orientation-selective neurons, each normalized to their preferred orientation (noted as 0°). Error bars, +s.d. **g, h**, Two-photon imaging of dendritic calcium signals in basal and oblique dendrites of another layer 2/3 neuron during action potential firing (electrical recording lower red trace) evoked by drifting gratings. **g**, Average image of 100 frames recorded at 173 μm below the cortical surface. Yellow dashed lines indicate out-of-focus portions of the dendrites. Green dashed lines indicate the regions of interest (ROIs). **h**, Ca^{2+} -dependent fluorescence changes (black traces) recorded in the soma and in five dendrites (indicated by numbers in **g**) and the corresponding membrane potential (V_m , red traces) recordings, during two separate trials. Light grey bars indicate the stimulation period with oriented gratings. AP, action potential.

calcium signalling in conditions in which we actively hyperpolarized the neurons.

Subthreshold calcium signals in dendritic hotspots

Figure 2 illustrates the results of an experiment in which a neuron was hyperpolarized to -70 mV to prevent action potential firing. In these conditions, a calcium transient was evoked in a subregion of 'dendrite 3' (Fig. 2a, b) by visual stimulation (drifting grating), but not detected in the other dendrites or in the soma. To assess the spatial dimensions of such local calcium transients, we analysed experiments



in which long portions of the same dendrite were discernible in the plane of focus of our recordings. In the neuron shown in Fig. 2c, we identified two dendritic hotspots of visually evoked local calcium transients. The systematic analysis of segments with a length of $3\ \mu\text{m}$ along the dendrite showed that the calcium signal was present in three neighbouring segments with a clear peak in the middle segment (Fig. 2c, d). Repetitive visual stimulation reliably evoked local dendritic calcium signals (Fig. 2e; mean failure rate $22 \pm 18\%$, 61 hotspots in 17 neurons). The spatial extent of these dendritic hotspots had an average half-width at half-maximum (HWHM) of $3.7 \pm 0.8\ \mu\text{m}$ ($n = 50$) (Fig. 2f).

What is the mechanism underlying these calcium signals? First, we noticed that the NMDA (*N*-methyl-D-aspartate) receptor antagonist D(-)-2-amino-5-phosphonvaleric acid (AP5) caused a major attenuation of the calcium transients, indicating their synaptic origin (Fig. 2g, h). Second, the dimensions of the hotspots were quite similar to the active dendritic shaft segments of pyramidal neurons *in vitro* displaying calcium transients as a result of the spread of calcium from single active spines^{34,35}. In line with this possibility, we also identified spines at the hotspot region when constructing post hoc ‘super-average’ images (Fig. 2c bottom). Furthermore, previous recordings performed in basal dendrites of neocortical neurons *in vitro*

Figure 2 | Subthreshold local dendritic calcium signals evoked by drifting grating stimulation. **a**, Two-photon image used for calcium recordings in **b**. The image is an average of 100 frames. Five ROIs are indicated by green dashed rectangles. **b**, Subthreshold Ca^{2+} transients (black traces) and corresponding depolarization (blue traces) evoked by drifting grating stimulation. Note the prominent Ca^{2+} signal in dendrite 3. Left traces, single trials; right traces, average (black trace) of five individual trials (grey traces) from various dendritic sites and soma, as indicated. **c**, Upper panel, pseudo-colour image of local dendritic Ca^{2+} signals. Ratio of the averages of 30 frames before and 30 frames during stimulation. Yellow arrows indicate two sites of local dendritic calcium signals. Lower panel, enlarged view of the dashed box indicated in the upper image, ‘super-average’ obtained from 500 frames. **d**, Calcium recordings from five neighbouring dendritic regions of $3\ \mu\text{m}$ length (d1–d5, ROIs shown in **c**), average of five trials. **e**, Calcium signals evoked during five consecutive trials within the ROI indicated by the red dashed line in **c**. **f**, Amplitude distribution of calcium signals within dendritic hotspots ($n = 50$ hotspots, 17 neurons). Grey dashed lines indicate the Gaussian fitting to the amplitude distribution of calcium signals within individual hotspots. Red line indicates the Gaussian fit to all points. Average half-width at half-maximum (HWHM) with standard deviation (\pm) is indicated. **g**, Left, two-photon image of a neuron (average $n = 100$ frames) and schematic representation of drug application pipette containing AP5 and Alexa-594. The red dashed lines indicate the approximate area of drug application. The green dashed box is the ROI for calcium monitoring. Right, Ca^{2+} recordings before, during and after the application of AP5. Average trace (black line) of five individual trials (grey lines). **h**, Amplitude of calcium signals before and during the application of AP5 obtained from $n = 9$ local calcium signals in four neurons. The amplitude of each Ca^{2+} signal was normalized to the mean amplitude of all signals in control condition. Paired *t*-test, *** $P < 0.0001$.

demonstrated that focally evoked subthreshold excitatory post-synaptic potentials induce calcium transients in dendritic compartments of comparable dimensions¹⁴. In our recordings, the mean amplitude of hotspot calcium transients (Methods) was $\Delta f/f = 0.25 \pm 0.07$ ($n = 50$). This value is comparable to the amplitudes of back-propagating action-potentials-dependent dendritic calcium transients evoked by the preferred orientation ($\Delta f/f = 0.37 \pm 0.13$, mean number of action potentials 3.1 ± 1.1 , $n = 50$; Supplementary Fig. 1c). Thus, the amplitude and the spatial extent of these visually evoked calcium transients resemble those generated by individual synaptic inputs, but not those evoked by dendritic NMDA spikes, which produce calcium transients that cover larger dendritic domains and have manifold larger amplitudes^{31,36,37}.

Mapping dendritic distribution of sensory inputs

To determine the spatial distribution of the dendritic hotspots reflecting sensory inputs, we performed experiments in which we attempted to image as many focal planes as possible in every neuron, requiring 1–2 h of whole-cell recording. In each focal plane, we determined the orientation preference of the local calcium signals by presenting drifting gratings (Methods). Figure 3a illustrates an experiment in which four focal planes were imaged at various depths under the cortical surface. A total of 13 hotspots were identified in this neuron. Figure 3b shows the response from three selected hotspots (numbered 4, 12 and 7 in Fig. 3a) obtained during presentation of eight directions of drifting gratings. From these averaged calcium transients ($n = 6$ trials), we constructed polar plots for each hotspot (Fig. 3c). A closer inspection of the polar plots revealed the presence of multiple orientation preferences in this and all other neurons. The dendritic distribution of the orientation preferences did not appear to follow any strict rule, but seemed to be randomly distributed throughout the dendritic tree. Another remarkable finding is that the calcium transients of most local dendritic hotspots displayed a pronounced orientation preference. In order to quantify the tuning level, we calculated the OSI for each hotspot and found that the majority of hotspots (72%, $n = 102$) were highly tuned for a particular orientation (OSI > 0.5). The average OSI value for all hotspots of the neuron shown in Fig. 3 was 0.63. Comparable results were obtained from 16 additional neurons (mean OSI = 0.59; $n = 102$

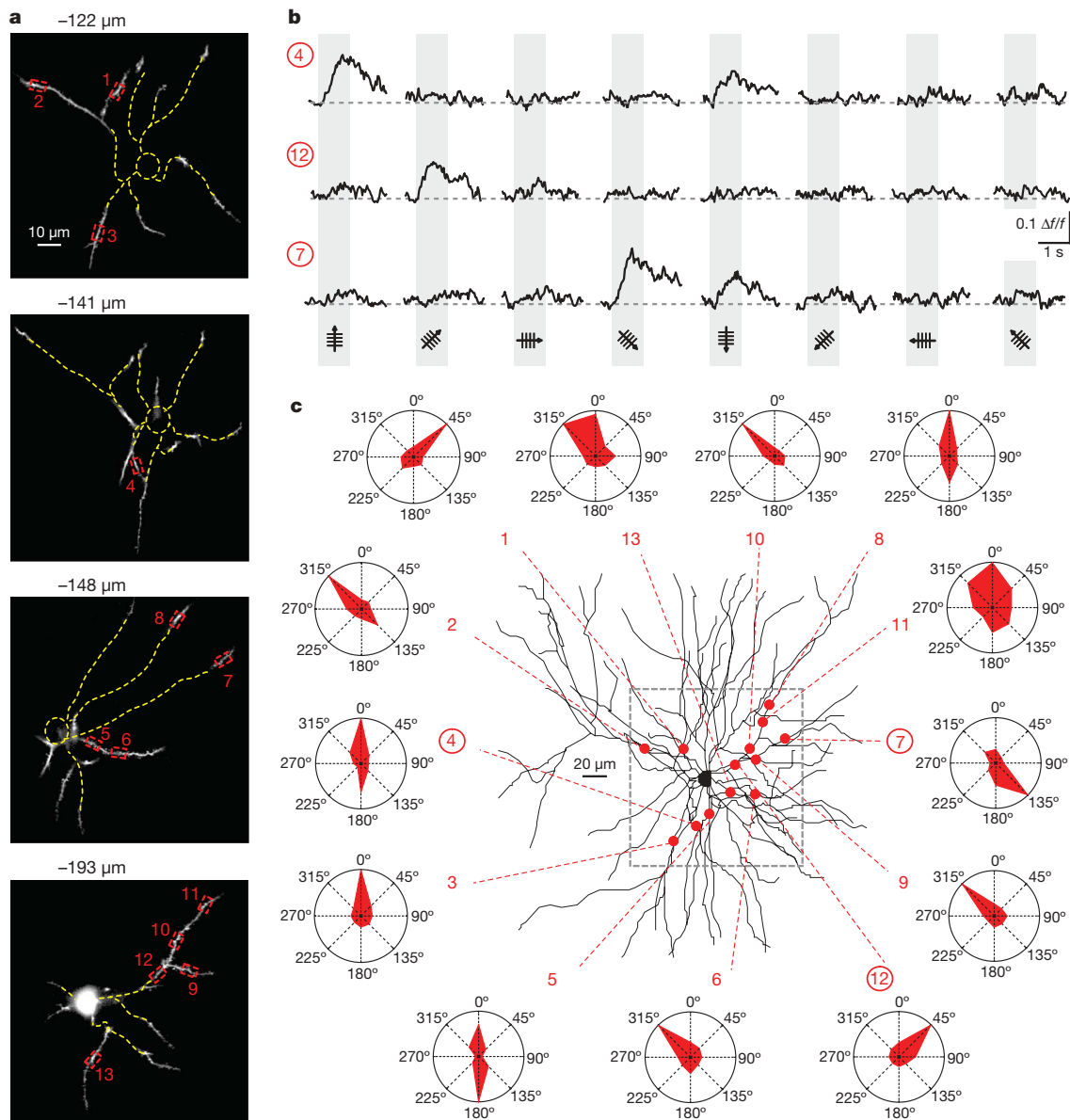


Figure 3 | Heterogeneity and distribution pattern of orientation-tuned dendritic hotspots. **a**, Four two-photon images (each an average of $n = 100$ frames) of a layer 2/3 neuron obtained at different depths under the cortical surface as indicated. Red dashed boxes indicate hotspots of local dendritic calcium signalling. **b**, Local dendritic calcium signals evoked by drifting gratings of different orientations (average of six trials) at three different

dendritic sites indicated in **a**. **c**, Location of each hotspot indicated as a red dot on the Z-projection of the reconstructed dendritic tree. Red dashed lines point to the polar plot obtained for the corresponding local Ca^{2+} signals. The frame (grey dashed line) indicates the area of imaging. The output signal of the neuron was tuned for the vertical orientation.

hotspots). An important finding was that dendritic hotspots were found in each of the recorded neurons (17/17), regardless of the tuning level of action potential firing and even in the neurons that were not reliably firing in response to drifting gratings. This suggests that these hotspots represent a general and highly reliable feature of layer 2/3 neurons of the primary visual cortex.

Hotspots of the same orientation preference in a given neuron were found widely dispersed over various dendrites. For example, in the neuron shown in Fig. 4a left, we identified six hotspots for the stimulus orientation indicated in the figure and, remarkably, each hotspot was on a different dendritic branch. The analysis of a larger set of neurons ($n = 8$, Fig. 4a right) confirmed this widespread distribution and emphasized the absence of any clustering of inputs on single dendrites. Furthermore, hotspots coding for the same orientation were found throughout the entire three-dimensional space surrounding the cell body. A similar wide distribution was observed for all four orientations tested (Supplementary Fig. 2). The absence of input

clustering became particularly obvious when we analysed the inputs to individual dendritic branches. Figure 4b shows three examples of dendritic branches with neighbouring hotspots that have different orientation preferences. In 9/10 dendritic branch segments, localized between two branching points, we encountered two or three hotspots tuned for different orientation preferences. In just one out of these 10 cases, neighbouring hotspots coded for the same orientation. The graph in Fig. 4c right summarizes these results. The left panel of Fig. 4c shows that all 'full dendrites', that is, individual dendrites together with all their higher order branches, received inputs for multiple orientations. Finally, we compared in 12 neurons the tuning levels of the firing pattern, representing the output signal, with the tuning levels of local dendritic calcium responses, representing the synaptic input signals. Experimentally, the orientation preference of spike firing in these neurons was determined during the initial 25–30 min of whole-cell recording during which the calcium indicator dye was allowed to equilibrate in the dendrites. Then, the neurons

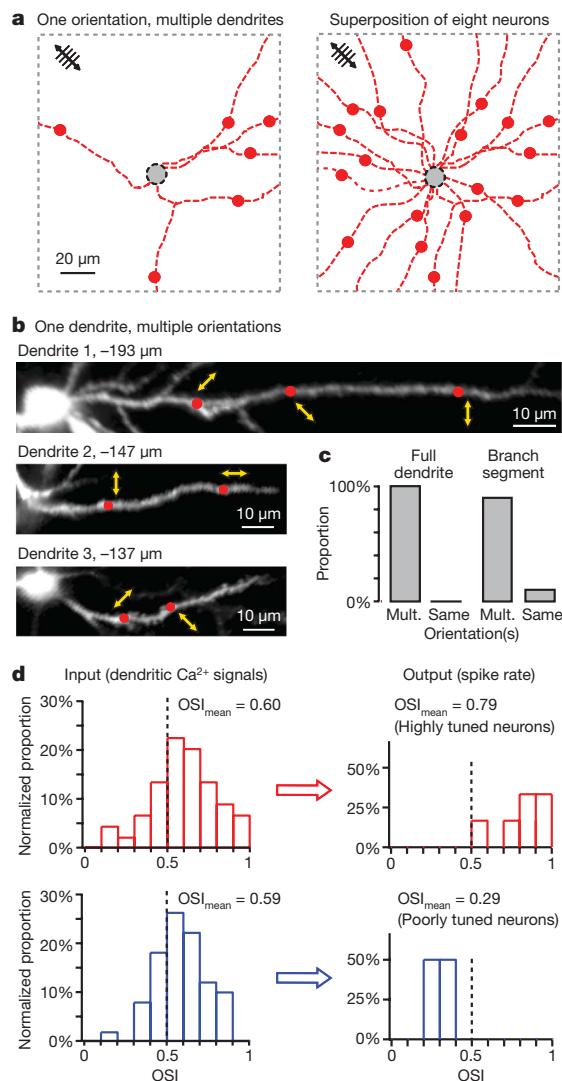


Figure 4 | Spatial arrangement of dendritic hotspots and input–output relation. **a**, Distribution of dendritic hotspots (red dots) tuned for the orientation preference indicated in the upper left corner, in the dendritic tree of a neuron (left panel). Right panel, summary of the results obtained for the same orientation in eight neurons. Cell bodies are indicated by the grey-filled dashed circles (black), dendrites are indicated by dashed red lines (Z-projections reconstructed from stacks). **b**, Three two-photon images of dendrites (each an average of $n = 100$ frames) at higher magnification with hotspots as indicated. Yellow arrows indicate the preferred orientation of local calcium signal in the corresponding hotspot. Note that the hotspots in dendrites 2 and 3 as well as the two distal hotspots in dendrite 1 were located in branch point-delimited segments. **c**, Summary graphs. Left panel, the proportion of full dendrites ($n = 12$) with hotspots coding for multiple orientations versus those with just one and the same orientation (≥ 3 hotspots per full dendrite). Right panel, the proportion of branch segments (between two branching points) with hotspots coding for multiple orientations versus those with the same orientation (≥ 2 hotspots per branch, $n = 10$). **d**, Input–output relations in highly tuned (upper) and poorly tuned (lower) neurons. The red and blue histograms show orientation selectivity indices (OSIs as indicated) for the input (Ca^{2+} signals in dendritic hotspots) and the output (spiking rate) of highly and poorly tuned neurons ($n = 6$ for each group), respectively.

were hyperpolarized and we determined the orientation preference of local dendritic calcium signals. We compared six highly tuned neurons (mean OSI = 0.79) with six broadly tuned ones (mean OSI = 0.29) (Fig. 4d right). Unexpectedly, the input signals had very similar tuning levels for the two neuronal groups, with mean OSI values of 0.60 and 0.59, for highly and broadly tuned firing patterns, respectively. This disparity between input and output signals, combined with

the above-mentioned observation that all neurons had input signals coding for multiple orientations, indicates that the orientation preference of the output signal is the result of a computational process taking place on the level of individual neurons.

Conclusions

Our results reveal basic insights into the dendritic organization of sensory inputs to neurons of the visual cortex *in vivo*. First, we identified discrete dendritic hotspots as synaptic entry sites for specific sensory features. These hotspots represent novel dendritic calcium signals *in vivo* and were found in all layer 2/3 neurons, irrespective of their output firing pattern. Second, we showed that afferent sensory inputs with the same orientation preference are widely dispersed over the dendritic tree and do not converge on single dendrites, as repeatedly proposed in recent years (see review in ref. 11 and references therein). Third, we found that even neurons with a highly tuned output signal receive input signals that are heterogeneous and code for multiple orientations and/or directions. Thus, taken together, our results support a neuronal integration model involving summation of distributed inputs, rather than models that stress the role of convergent inputs to single dendrites^{6,15}. However, it is certainly possible that other types of cortical neurons, especially those with pronounced apical tufts³⁸ or neurons in other species with a columnar organization of the visual cortex^{17,19–21}, have more clustered sensory inputs to the same dendrite, capable of generating large amplitude dendritic spikes^{6,11}. The approach introduced in this study opens the way to a detailed analysis of various types of neurons followed by the construction of functional wiring diagrams of sensory pathways with single input resolution *in vivo*.

METHODS SUMMARY

C57BL/6 mice (postnatal day (P)28–P34) were prepared for *in vivo* two-photon calcium imaging and whole-cell recordings under isoflurane anaesthesia as described previously³⁹. Whole-cell patch-clamp recordings of layer 2/3 neurons of primary visual cortex (monocular region) were performed by ‘shadow-patching’²⁵. Neurons were dialysed with a pipette solution containing the fluorescent Ca^{2+} indicator Oregon green BAPTA-1 hexapotassium (OGB-1; 100 μM), Alexa-594 (25 μM) and biocytin (2 mg ml^{-1}). Basal and oblique dendrites that appeared on the same focal plane were imaged by high-speed two-photon microscopy involving a resonant galvo-scanner³⁰. Membrane potential changes and Ca^{2+} signals were simultaneously recorded. The focal plane depth and the imaged area were chosen to contain as many dendrites as possible. At each focal plane, we imaged the activity evoked by drifting square wave gratings (0.03 cycles per degree, 1 Hz, eight directions, standing phase 2 s, drifting phase 1 s). Transient changes in Ca^{2+} fluorescence ($\Delta f/f$) were systematically examined by an adaptive algorithm, which involved small regions of interest (ROIs) of $3 \times 4 \mu\text{m}$, noise filtering and pattern matching. The NMDA receptor antagonist AP5 (together with Alexa-594) was locally applied by pressure ejection close to the imaged dendrites. The spread of the ejected solution was monitored by imaging Alexa fluorescence. The tuning level of local dendritic calcium signals with regard to the orientation of the drifting grating was quantified by an OSI²⁴.

Received 14 October 2009; accepted 24 February 2010.

1. London, M. & Häusser, M. Dendritic computation. *Annu. Rev. Neurosci.* **28**, 503–532 (2005).
2. Bloodgood, B. L. & Sabatini, B. L. Ca^{2+} signaling in dendritic spines. *Curr. Opin. Neurobiol.* **17**, 345–351 (2007).
3. Markram, H. & Sakmann, B. Calcium transients in dendrites of neocortical neurons evoked by single subthreshold excitatory postsynaptic potentials via low-voltage-activated calcium channels. *Proc. Natl Acad. Sci. USA* **91**, 5207–5211 (1994).
4. Nevian, T. & Sakmann, B. Spine Ca^{2+} signaling in spike-timing-dependent plasticity. *J. Neurosci.* **26**, 11001–11013 (2006).
5. Yuste, R. & Denk, W. Dendritic spines as basic functional units of neuronal integration. *Nature* **375**, 682–684 (1995).
6. Häusser, M. & Mel, B. Dendrites: bug or feature? *Curr. Opin. Neurobiol.* **13**, 372–383 (2003).
7. Helmchen, F., Svoboda, K., Denk, W. & Tank, D. W. *In vivo* dendritic calcium dynamics in deep-layer cortical pyramidal neurons. *Nature Neurosci.* **2**, 989–996 (1999).
8. Murayama, M. *et al.* Dendritic encoding of sensory stimuli controlled by deep cortical interneurons. *Nature* **457**, 1137–1141 (2009).

9. Svoboda, K., Denk, W., Kleinfeld, D. & Tank, D. W. *In vivo* dendritic calcium dynamics in neocortical pyramidal neurons. *Nature* **385**, 161–165 (1997).
10. Johnston, D. & Narayanan, R. Active dendrites: colorful wings of the mysterious butterflies. *Trends Neurosci.* **31**, 309–316 (2008).
11. Larkum, M. E. & Nevian, T. Synaptic clustering by dendritic signalling mechanisms. *Curr. Opin. Neurobiol.* **18**, 321–331 (2008).
12. Ohki, K. & Reid, R. C. Specificity and randomness in the visual cortex. *Curr. Opin. Neurobiol.* **17**, 401–407 (2007).
13. Magee, J. C. Dendritic integration of excitatory synaptic input. *Nature Rev. Neurosci.* **1**, 181–190 (2000).
14. Polsky, A., Mel, B. W. & Schiller, J. Computational subunits in thin dendrites of pyramidal cells. *Nature Neurosci.* **7**, 621–627 (2004).
15. Cash, S. & Yuste, R. Linear summation of excitatory inputs by CA1 pyramidal neurons. *Neuron* **22**, 383–394 (1999).
16. Bannister, A. P. Inter- and intra-laminar connections of pyramidal cells in the neocortex. *Neurosci. Res.* **53**, 95–103 (2005).
17. Hirsch, J. A. & Martinez, L. M. Laminar processing in the visual cortical column. *Curr. Opin. Neurobiol.* **16**, 377–384 (2006).
18. Svoboda, K., Helmchen, F., Denk, W. & Tank, D. W. Spread of dendritic excitation in layer 2/3 pyramidal neurons in rat barrel cortex *in vivo*. *Nature Neurosci.* **2**, 65–73 (1999).
19. Hubel, D. H. & Wiesel, T. N. Receptive fields, binocular interaction and functional architecture in the cat's visual cortex. *J. Physiol. (Lond.)* **160**, 106–154 (1962).
20. Hubel, D. H. & Wiesel, T. N. Receptive fields and functional architecture of monkey striate cortex. *J. Physiol. (Lond.)* **195**, 215–243 (1968).
21. White, L. E. & Fitzpatrick, D. Vision and cortical map development. *Neuron* **56**, 327–338 (2007).
22. Dräger, U. C. Receptive fields of single cells and topography in mouse visual cortex. *J. Comp. Neurol.* **160**, 269–290 (1975).
23. Métin, C., Godement, P. & Imbert, M. The primary visual cortex in the mouse: receptive field properties and functional organization. *Exp. Brain Res.* **69**, 594–612 (1988).
24. Niell, C. M. & Stryker, M. P. Highly selective receptive fields in mouse visual cortex. *J. Neurosci.* **28**, 7520–7536 (2008).
25. Kitamura, K., Judkewitz, B., Kano, M., Denk, W. & Häusser, M. Targeted patch-clamp recordings and single-cell electroporation of unlabeled neurons *in vivo*. *Nature Methods* **5**, 61–67 (2008).
26. Kerr, J. N., Greenberg, D. & Helmchen, F. Imaging input and output of neocortical networks *in vivo*. *Proc. Natl Acad. Sci. USA* **102**, 14063–14068 (2005).
27. Anderson, J., Lampl, I., Reichova, I., Carandini, M. & Ferster, D. Stimulus dependence of two-state fluctuations of membrane potential in cat visual cortex. *Nature Neurosci.* **3**, 617–621 (2000).
28. Carandini, M. & Ferster, D. Membrane potential and firing rate in cat primary visual cortex. *J. Neurosci.* **20**, 470–484 (2000).
29. Bringuier, V., Chavane, F., Glaeser, L. & Fregnac, Y. Horizontal propagation of visual activity in the synaptic integration field of area 17 neurons. *Science* **283**, 695–699 (1999).
30. Rochefort, N. L. *et al.* Sparsification of neuronal activity in the visual cortex at eye-opening. *Proc. Natl Acad. Sci. USA* **106**, 15049–15054 (2009).
31. Gordon, U., Polsky, A. & Schiller, J. Plasticity compartments in basal dendrites of neocortical pyramidal neurons. *J. Neurosci.* **26**, 12717–12726 (2006).
32. Koester, H. J. & Sakmann, B. Calcium dynamics associated with action potentials in single nerve terminals of pyramidal cells in layer 2/3 of the young rat neocortex. *J. Physiol. (Lond.)* **529**, 625–646 (2000).
33. Bollmann, J. H. & Engert, F. Subcellular topography of visually driven dendritic activity in the vertebrate visual system. *Neuron* **61**, 895–905 (2009).
34. Kovalchuk, Y., Eilers, J., Lisman, J. & Konnerth, A. NMDA receptor-mediated subthreshold Ca²⁺ signals in spines of hippocampal neurons. *J. Neurosci.* **20**, 1791–1799 (2000).
35. Noguchi, J., Matsuzaki, M., Ellis-Davies, G. C. & Kasai, H. Spine-neck geometry determines NMDA receptor-dependent Ca²⁺ signaling in dendrites. *Neuron* **46**, 609–622 (2005).
36. Holthoff, K., Kovalchuk, Y., Yuste, R. & Konnerth, A. Single-shock LTD by local dendritic spikes in pyramidal neurons of mouse visual cortex. *J. Physiol. (Lond.)* **560**, 27–36 (2004).
37. Major, G., Polsky, A., Denk, W., Schiller, J. & Tank, D. W. Spatiotemporally graded NMDA spike/plateau potentials in basal dendrites of neocortical pyramidal neurons. *J. Neurophysiol.* **99**, 2584–2601 (2008).
38. Larkum, M. E., Nevian, T., Sandler, M., Polsky, A. & Schiller, J. Synaptic integration in tuft dendrites of layer 5 pyramidal neurons: a new unifying principle. *Science* **325**, 756–760 (2009).
39. Stosiek, C., Garaschuk, O., Holthoff, K. & Konnerth, A. *In vivo* two-photon calcium imaging of neuronal networks. *Proc. Natl Acad. Sci. USA* **100**, 7319–7324 (2003).

Supplementary Information is linked to the online version of the paper at www.nature.com/nature.

Acknowledgements We are grateful to B. Sakmann for discussions and to Y. Kovalchuk for help in the initial experiments. This work was supported by grants from the DFG (to A.K.) and the Friedrich Schiedel Foundation. A.K. is a Carl von Linde Senior Fellow of the Institute for Advanced Study of the TUM. H.J., N.L.R. and X.C. were supported by the DFG (IRTG 1373).

Author Contributions H.J., N.L.R. and X.C. carried out the experiments. H.J., N.L.R. and A.K. performed the analysis. A.K. designed the study and wrote the manuscript with the help of all authors.

Author Information Reprints and permissions information is available at www.nature.com/reprints. The authors declare no competing financial interests. Correspondence and requests for materials should be addressed to A.K. (arthur.konnerth@lrz.tum.de).